Analysis of heterogeneous Markov media for particle transport problems

Mikolaj Adam Kowalski ⬤,[*] Coline Larmier,[†] and Andrea Zoia ⬤[‡]

Université Paris-Saclay, CEA, Service d'études des réacteurs et de mathématiques appliquées, 91191 Gif-sur-Yvette, France

Markov media provide a prototype class of stochastic geometries that are widely used in order to model several complex and disordered systems encompassing, e.g., turbulent fluids and plasma, atmospheric layers, or biological tissues, especially in relation to particle transport problems. In several key applications, the statistical properties of random media may display spatial gradients due to material stratification, which means that the typical spatial scale and the probability of finding a given material phase at a spatial location become nonhomogeneous. In this paper we investigate the main features of spatially heterogeneous Markov media, using Poisson hyperplane tessellations and Arak polygonal fields. We show that both models can generate geometry realizations sharing Markov-like properties, and discuss their distinct advantages and drawbacks in terms of flexibility and ease of use. The impact of these models on the observables related to particle transport will be assessed using Monte Carlo simulations.

I. INTRODUCTION

Random media are ubiquitous models that emerge in several applications in physics and life sciences [1], in particular in relation to particle transport problems [2]. Examples are widespread and concern, for instance, photon and ion propagation through Rayleigh-Taylor turbulent layers in inertial confinement fusion [3–6], radiative transfer in turbid materials [7–9], or neutron transport in randomly dispersed fuel lumps and absorbers [10–14], to name a few. The material properties of stochastic media at a given position are known only statistically. To fix the ideas, we will assume that a finite set of N immiscible phases with label $\alpha = \{0, 1, \ldots, N-1\}$ can be present at a given point,[1] and we denote by $p_\alpha(\mathbf{r})$ the probability of finding phase α at position $\mathbf{r}$ [2]. In order to characterize d-dimensional random media, a key question concerns the degree of correlation between the phases present at various points, which can be typically assessed via stereological methods by estimating the covariance between material phases at positions $\{\mathbf{r}, \mathbf{r}'\}$ along d^*-dimensional sections, with $d^* \leqslant d$. In particular, it has been shown that the statistical features of random media are intimately related to the distribution of one-dimensional sections, which can be inferred from the probability density $f_\alpha(s|\mathbf{r}, \mathbf{\Omega})$ of the chord length s determined by intersecting an arbitrary line of orientation $\mathbf{\Omega}$ at position $\mathbf{r}$ with the boundaries of a material chunk of phase α [1]. Knowledge of $f_\alpha(s|\mathbf{r}, \mathbf{\Omega})$ is especially valuable for particle transport problems, since it allows inferring the effects of the random material structure on the particle trajectories

[2]. In this respect, Markov media provide an idealized mathematical model for complex disordered materials, demanding minimal information content: chord lengths are assumed to obey the nonhomogeneous exponential distribution

$$f_\alpha(s|\mathbf{r}, \mathbf{\Omega}) = \rho_\alpha(\mathbf{r} + s\mathbf{\Omega}, \mathbf{\Omega})e^{-\int_0^s \rho_\alpha(\mathbf{r}+s'\mathbf{\Omega}, \mathbf{\Omega})\, ds'}, \qquad (1)$$

where the parameter $\rho_\alpha(\mathbf{r}, \mathbf{\Omega})$ represents the probability per unit length to leave material α in direction $\mathbf{\Omega}$ at position $\mathbf{r}$ [2]. The material probabilities $p_\alpha(\mathbf{r})$ are related to the rates $\rho_\alpha(\mathbf{r}, \mathbf{\Omega})$ through the Chapman-Kolmogorov equation, which is basically a probability conservation law [2]. In addition to providing a prototype reference model that can be usefully adopted to benchmark annealed-disorder approaches [15,16], Markov media offer a fairly accurate description of real-world turbulent fluids and plasma, despite their highly simplified nature; for a review, see, e.g., [9,17,18].

In the context of particle transport, Markov media satisfying Eq. (1) were first introduced in one-dimensional settings, where the corresponding material realizations can be sampled by a Markov jump process along a line [2], and extensively investigated for the case of spatially homogeneous statistics [19,20]. A faithful description of many realistic applications, such as density-driven material stratification in turbulent mixing, requires to take into account the presence of spatial gradients: generally speaking, the statistical properties of the stochastic media will depend on the space position. Heterogeneity can be introduced in two distinct ways: by the spatial scale and by the material probability. For one-dimensional Markov media, this can be achieved by using space-dependent parameters in the underlying Markov jump process along the line, which allows separately controlling a gradient in the spatial scale and in the material probability [21–23].

The practical feasibility of generalizing Markov media to higher dimensions, which is of utmost importance to model real-world systems, has been long debated [3,24–26]. Switzer

---

[*]mikolaj-adam.kowalski@cea.fr

[†]coline.larmier@cea.fr

[‡]andrea.zoia@cea.fr

[1]We follow the usual convention in Pomraning, where the numbering of the material phases starts from $\alpha = 0$ [2].

exhibited a pioneering example of spatially homogeneous and isotropic random media in dimension $d = 2$ having Markov line transects, via a two-step approach based on first sampling random polygons using a Poisson line process and then attributing each polygon a phase ("color") with independent probability [27]: such construction was then used for particle transport applications [28,29]. Switzer's procedure has been later extended to dimension $d = 3$ (and beyond) [15,30] using homogeneous and isotropic Poisson hyperplane tessellations, a powerful tool of stochastic geometry [31]. Building on these findings, further generalizations to nonisotropic [32] and spatially heterogeneous d-dimensional Markov media [33] have been recently proposed.

In this work, we revisit higher-dimensional Markov media for particle transport problems, with a twofold aim. First, we illustrate the main statistical features of the stochastic geometries built using Switzer's procedure, in a general space-dependent and nonisotropic setting. In particular, we will point out that Switzer's procedure can yield heterogeneity in the spatial scale but not in the material probability, which somewhat restrains the kind of spatial gradients of the material properties that can be modeled by this class of Markov media. Second, we will show that other models exist satisfying Eq. (1) and being amenable to an explicit construction: the broad class of Arak's polygonal mosaics, e.g., exhibits a stronger spatial Markov property in addition to the line-Markov property [34–37]. The family of Arak's models, although requiring a much more cumbersome sampling than Poisson tessellations, can be extended to accommodate spatial gradients in both the spatial scale and the material probability.

This paper is organized as follows: in Sec. II we will present a brief review of Markov media on a line. In Sec. III we will introduce higher-dimensional spatially heterogeneous Markov media obtained by the Switzer's procedure, and discuss their statistical properties. In Sec. IV we will then address the homogeneous and isotropic Arak's polygonal mosaics and show how they can be extended to include spatial gradients in the spatial scale and/or the material probability. Finally, in Sec. V we will compare the features of Switzer-based and Arak-based Markov media with respect to particle transport problems, using Monte Carlo simulations to support our investigations. Conclusions will be drawn in Sec. VI.

II. REVIEW OF MARKOV MIXING ON A LINE

We begin by recalling the basic features of Markov media on a line, a prototype model that will be used as a reference for the higher-dimensional generalizations discussed in the next sections.

A. Construction based on sweeping

Consider a line populated with a finite collection of N random materials ("colors"), each associated to a discrete index $\alpha = \{0, 1, \dots, N-1\}$, and define the stochastic process $(\mathcal{C}_x)_{x \geqslant x_0}$ whose family of random variables yields the color $C(x)$ at position $x \geqslant x_0$ along the line. Multimaterial Markov statistics on a line are specified by assigning the Poisson transition rates $\rho_{\alpha,\beta}(x, \Omega_+)$, denoting the probability per unit length to have a transition from material α to material $\beta \neq \alpha$
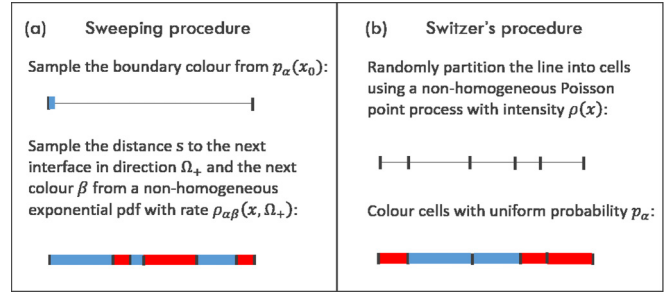

FIG. 1. Monte Carlo sampling of one-dimensional Markov media on a line. (a) Scheme based on sweeping using (oriented) transition rates $\rho_{\alpha,\beta}(x, \Omega_\pm)$ between colors. (b) The Switzer procedure, based on a Poisson point process with density $\rho(x)$ and independent coloring probabilities.

at position x, together with the probability $p_\alpha(x_0)$ of having color α at $x = x_0$ [2,22]. The quantities $\rho_{\alpha,\beta}(x, \Omega_+)$ are in general space-dependent, and the symbol Ω_+ is reminiscent of the fact that the transition rates are taken in the direction of increasing x. The transition rates satisfy $\rho_{\alpha,\beta}(x, \Omega_+) \geqslant 0$ for $\beta \neq \alpha$, and we set $\rho_{\alpha,\alpha}(x, \Omega_+) = 0$. Knowledge of $\rho_{\alpha,\beta}(x, \Omega_+)$ and $p_\alpha(x_0)$ enables a Monte Carlo strategy to sample an ensemble of Markov media, using, e.g., Gillespie's algorithm [38]: one would "sweep" the line from left to right by adding the random material segment lengths, starting from the initial condition at x_0. For visualization, the sweeping procedure is illustrated in Fig. 1(a).

Several exact formulas for one-dimensional Markov statistics can be obtained by transposing well-known results from time-dependent Markov processes, mapping the time variable into the space coordinate along the line [2,22]. We will denote by

$$\rho_\alpha(x, \Omega_+) = \sum_{\beta \neq \alpha} \rho_{\alpha,\beta}(x, \Omega_+) \qquad (2)$$

the rate at which material α is abandoned. By construction, the probability density of having a chord of length s in material α at the right of point x obeys

$$f_\alpha(s|x, \Omega_+) = \rho_\alpha(x + s, \Omega_+) e^{-\int_0^s \rho_\alpha(x+s', \Omega_+) ds'}, \qquad (3)$$

which is the one-dimensional equivalent of Eq. (1). The memory-less nature of the chord length distribution in Eq. (3) induces the following spatial Markov property: given a collection of n ordered points $x_1, x_2, \dots, x_n$ along the line, for the color probabilities we have

$$\mathcal{P}(C_n|C_{n-1}, \dots, C_2, C_1) = \mathcal{P}(C_n|C_{n-1}), \qquad (4)$$

where C_i is the color at point x_i, $i = 1, \dots, n$. We will further introduce the conditional transition probability $P_{\alpha,\beta}(x', x)$ of having material β at x given that $x' < x$ is in material α, which is related to the transition rates by

$$\rho_{\alpha,\beta}(x, \Omega_+) = \lim_{x' \to x} \frac{1}{x' - x} P_{\alpha,\beta}(x, x'). \qquad (5)$$

Based on the Markov property, $P_{\alpha,\beta}(x',x)$ obeys the Chapman-Kolmogorov equation

$$P_{\alpha,\beta}(x',x) = \sum_{\gamma} P_{\alpha,\gamma}(x',x'')P_{\gamma,\beta}(x'',x), \qquad (6)$$

for $x_0 \leqslant x' < x'' < x$, with the normalization $\sum_{\beta} P_{\alpha,\beta}(x',x) = 1$. By taking the derivative of Eq. (6) with respect to x and using the definition in Eq. (5), it can be shown that $P_{\alpha,\beta}(x',x)$ satisfies the forward Kolmogorov equation

$$\frac{\partial}{\partial x} P_{\alpha,\beta}(x',x) = \sum_{\gamma \neq \beta} P_{\alpha,\gamma}(x',x)\rho_{\gamma,\beta}(x,\Omega_+)$$
$$- P_{\alpha,\beta}(x',x)\rho_{\beta}(x,\Omega_+), \qquad (7)$$

with the initial condition $P_{\alpha,\beta}(x,x) = \delta_{\alpha,\beta}$. For the special case of binary media, with $N = 2$, the transition rates will only depend on the initial state, i.e., $\rho_{\alpha,\beta}(x,\Omega_+) = \rho_{\alpha}(x,\Omega_+)$ for $\beta \neq \alpha$, and the solution of Eq. (7) reads

$$P_{\alpha,\beta}(x',x) = \int_{x'}^{x} \rho_{\alpha}(z,\Omega_+)e^{-\int_z^x \hat{\rho}_2(u,\Omega_+)du}dz \qquad (8)$$

for $\beta \neq \alpha$, with $\hat{\rho}_2(x,\Omega_+) = \rho_0(x,\Omega_+) + \rho_1(x,\Omega_+)$, and $P_{\alpha,\alpha}(x',x) = 1 - P_{\alpha,\beta}(x',x)$. The solution of the N-ary case $N > 2$ could be solved by matrix exponential methods, although in practice closed-form results are typically out of reach. For binary mixtures, it has been suggested that the quantity $\hat{\rho}_2$ plays the role of the typical (inverse) spatial scale of the random media [2]; by analogy, it would be tempting to similarly use $\hat{\rho}_N = \sum_{\alpha} \rho_{\alpha}(x,\Omega_\pm)$ for $N > 2$. The color probability $p_{\alpha}(x)$ of having phase α at x follows from $P_{\alpha,\beta}(x',x)$: we set

$$p_{\alpha}(x) = \sum_{\beta} p_{\beta}(x_0)P_{\beta,\alpha}(x_0,x), \qquad (9)$$

with the normalization $\sum_{\alpha} p_{\alpha}(x) = 1$. Taking the derivative of Eq. (9) with respect to x and using the definitions above, $p_{\alpha}(x)$ satisfies the forward Kolmogorov equation

$$\frac{\partial}{\partial x} p_{\alpha}(x) = \sum_{\beta \neq \alpha} p_{\beta}(x)\rho_{\beta,\alpha}(x,\Omega_+) - p_{\alpha}(x)\rho_{\alpha}(x,\Omega_+). \quad (10)$$

Equations (10) form a system of N differential equations, to be solved with the initial condition at $x = x_0$. Similarly as for $P_{\alpha,\beta}(x',x)$, solutions to arbitrary N-ary cases are generally difficult to compute, but for $N = 2$ the solution is readily found:

$$p_{\alpha}(x) = \int_{x_0}^{x} \rho_{\beta}(z,\Omega_+)e^{-\int_z^x \hat{\rho}_2(u,\Omega_+)du}dz, \qquad (11)$$

with $p_{\beta}(x) = 1 - p_{\alpha}(x)$. Stationary solutions $p_{\alpha}(x) = \pi_{\alpha}$ to the system of Eqs. (10) may exist, provided that the transition rates satisfy

$$\sum_{\beta \neq \alpha} \pi_{\beta}\rho_{\beta,\alpha}(x,\Omega_+) = \pi_{\alpha}\rho_{\alpha}(x,\Omega_+) \qquad (12)$$

for any α, which implies $\partial_x p_{\alpha}(x) = 0$; if the initial condition $p_{\alpha}(x_0) \neq \pi_{\alpha}$, there will be a transient regime.

So far, we have assumed that the Markov statistics are induced by sweeping the line from left to right, using the transition rates $\rho_{\alpha,\beta}(x,\Omega_+)$. The line can equivalently be swept from right to left: we will denote by $\rho_{\alpha,\beta}(x,\Omega_-)$ the corresponding rates of transition from material α to material $\beta \neq \alpha$ in the direction of decreasing x. It can be shown that for Markov media a symmetry relation holds between forward- and backward-oriented rates [22], namely,

$$p_{\alpha}(x)\rho_{\alpha,\beta}(x,\Omega_\pm) = p_{\beta}(x)\rho_{\beta,\alpha}(x,\Omega_\mp) \qquad (13)$$

for $\beta \neq \alpha$, whence also

$$p_{\alpha}(x)\rho_{\alpha}(x,\Omega_\pm) = \sum_{\beta \neq \alpha} p_{\beta}(x)\rho_{\beta,\alpha}(x,\Omega_\mp). \qquad (14)$$

Using the symmetry property, Eq. (10) can be rewritten in terms of the backward-oriented rates as

$$-\frac{\partial}{\partial x} p_{\alpha}(x) = \sum_{\beta \neq \alpha} p_{\beta}(x)\rho_{\beta,\alpha}(x,\Omega_-) - p_{\alpha}(x)\rho_{\alpha}(x,\Omega_-). \qquad (15)$$

The chord length densities in the forward $f_{\alpha}(s|x,\Omega_+)$ and backward direction $f_{\alpha}(s|x,\Omega_-)$ are related by the following symmetry condition:

$$\sum_{\beta \neq \alpha} p_{\beta}(x)\rho_{\beta,\alpha}(x,\Omega_+)f_{\alpha}(s|x,\Omega_+)$$
$$= \sum_{\beta \neq \alpha} p_{\beta}(x+s)\rho_{\beta,\alpha}(x+s,\Omega_-)f_{\alpha}(s|x+s,\Omega_-), \quad (16)$$

which expresses a balance between the rate at which realizations enter material α at x and leave it at $x + s$ in the direction of positive x (the left-hand side) and the opposite rate at which realizations enter material α at $x + s$ and leave it at x in the direction of negative x (the right-hand side) [22]. A few significant examples of chord length distributions for spatially heterogeneous binary media are illustrated in Fig. 2, where the solutions of Eqs. (3) and (16) are compared with Monte Carlo simulations.

The transition rates $\rho_{\alpha,\beta}(x,\Omega_\pm)$ describe Markov line statistics with arbitrary spatial gradients. In the special case where the rates $\rho_{\alpha,\beta}(x,\Omega_\pm) = \rho_{\alpha,\beta}(\Omega_\pm)$ are spatially homogeneous, the corresponding mixing statistics are invariant under arbitrary translations,[2] which results in a simplification of the general formulas provided above. In particular, two-point probabilities $P_{\alpha,\beta}(x',x)$ will depend on the distance $x - x'$ alone, whereas the local quantities $p_{\alpha}(x)$ and $\rho_{\alpha}(x,\Omega_\pm)$ will be spatially constant. For the chord length distribution, invariance under translation combined with symmetry yields in particular

$$f_{\alpha}(s|\Omega_+) = f_{\alpha}(s|\Omega_-), \qquad (17)$$

which implies that the transition rates for spatially homogeneous statistics

$$\rho_{\alpha}(\Omega_+) = \rho_{\alpha}(\Omega_-) = \rho_{\alpha} \qquad (18)$$

do not depend on the sweeping direction (symmetry under reversal $\Omega_\pm \to \Omega_\mp$). The chord length distribution is thus the simple exponential density function $f_{\alpha}(s|\Omega_\pm) = \rho_{\alpha}\exp(-\rho_{\alpha}s)$. Furthermore, since $f_{\alpha}(s|\Omega_\pm)$ are spatially

_____

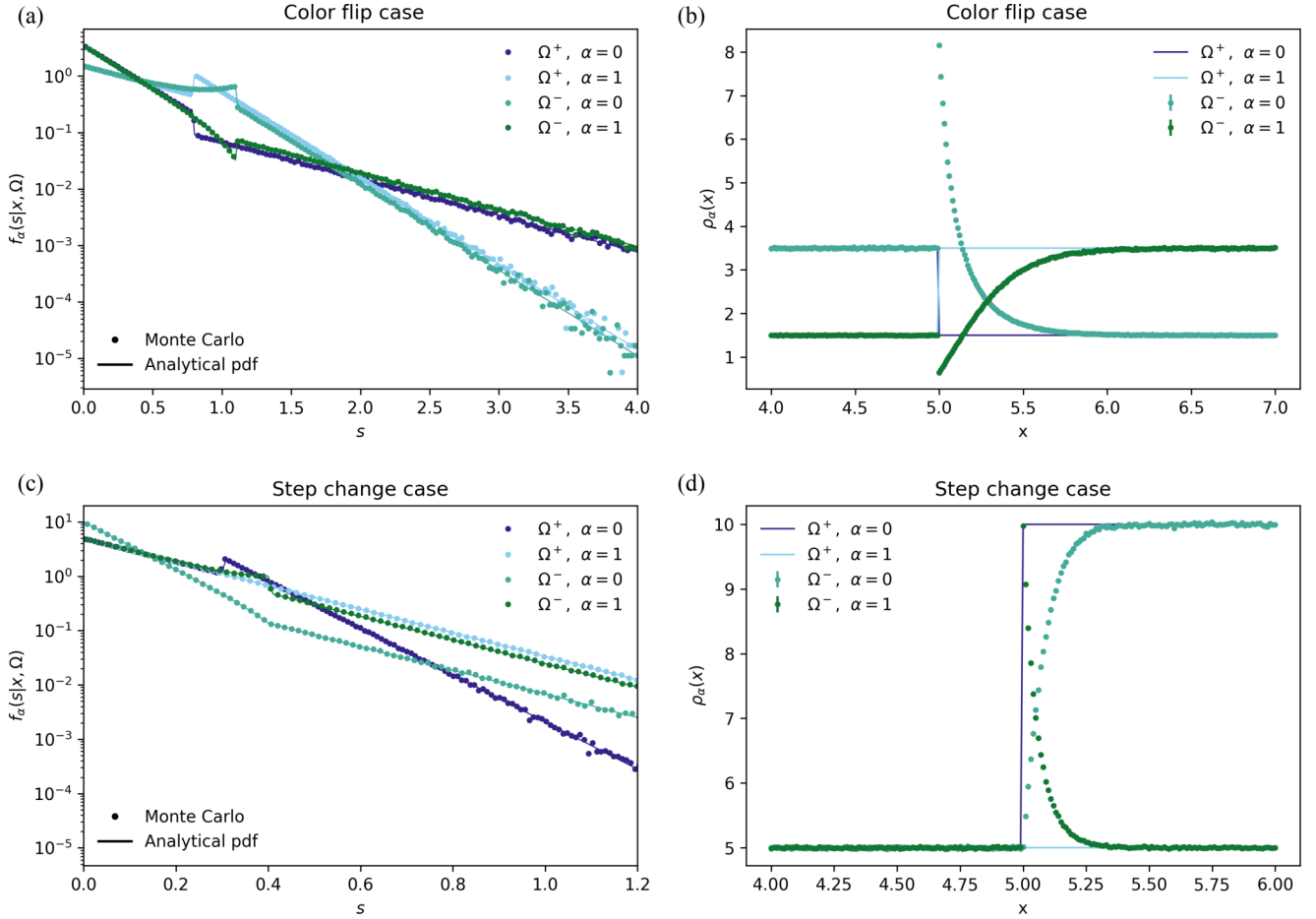[2]Provided that the initial condition $p_{\alpha}(x_0)$ is set accordingly.

FIG. 2. Statistical properties of one-dimensional heterogeneous binary Markov media on interval [0,10]. The "color flip" case in (a) and (b) represents an inversion of coloring probability, which initially was $p_0 = 0.3$ with $\rho = 5$. The "step change" case in (c) and (d) represents a change in both spatial scale and color achieved by a step increase of the transition rate ρ_0 for phase $\alpha = 0$. [(a), (c)] Comparison of the Monte Carlo histogram of the chord length distribution (symbols) against the solution of Eq. (3) (solid lines). For reversed direction Ω_-, the estimated transition rates were used in the nonhomogeneous exponential distribution. [(b), (d)] Corresponding transition rates (Monte Carlo estimates displayed as symbols; analytical formulas as solid lines). For the forward direction Ω_+, the exact chosen value of the rates is displayed, whereas for the reversed direction Ω_- the estimated value is displayed. Error bars (barely visible) represent one σ uncertainty. Chord lengths and transition rates were estimated based on independent sets of realizations.

constant, the quantity

$$\Lambda_\alpha = \frac{1}{\rho_\alpha} = \int_0^\infty s f_\alpha(s|\Omega_\pm) ds \qquad (19)$$

can be interpreted as the average chord length in material α. The color probability p_α satisfies the system of equations

$$p_\alpha \rho_\alpha = \sum_{\beta \neq \alpha} p_\beta \rho_{\beta,\alpha}(\Omega_\pm), \qquad (20)$$

with the constraints due to Eq. (2) and the normalization. For the case of binary statistics, the only solution for p_α is symmetrical, namely, $p_\alpha = \Lambda_\alpha/(\Lambda_0 + \Lambda_1)$. For the N-ary case with $N > 2$, symmetrical solutions $p_\alpha = \Lambda_\alpha / \sum_\alpha \Lambda_\alpha$ may exist provided that the transition rates satisfy the condition

$$\frac{\rho_{\alpha,\beta}(\Omega_\pm)}{\rho_\alpha} = \frac{\rho_{\beta,\alpha}(\Omega_\mp)}{\rho_\beta}. \qquad (21)$$

For arbitrary transition rates, however, the solutions for p_α will be generally speaking nonsymmetrical.

B. Construction based on colored tessellations

One-dimensional Markov media can be alternatively obtained using a two-step strategy that, although less general than the sweeping procedure, is preparatory to the extension to higher dimensions. The underlying idea is to first sample a stochastic partition (tessellation) of the line using a point process (the random points will define the boundaries of the tessellation cells), and then apply a Switzer's-like "coloring" procedure whereupon the tessellation cells are assigned a material label, in such a way that the resulting random media satisfy the Markov line property in Eq. (3). Perhaps the simplest way of achieving this goal is to use a one-dimensional Poisson point process with density $\rho(x)$, and then assign colors α to each cell with independent probabilities p_α. In this case, the colored line statistics will have a line-Markov property, with parameter $\rho_\alpha(x, \Omega_\pm) = \rho(x)(1 - p_\alpha)$. For visualization, the colored tessellation procedure is illustrated in Fig. 1(b).

Actually, the properties of this class of Markov media are more restrictive than those obtained using the sweeping

procedure. In particular, while spatial gradients can be generated through the space-dependent tessellation density $\rho(x)$, the color probability p_α is necessarily homogeneous, so that no color gradient effect can be taken into account. Furthermore, one-dimensional Poisson tessellations induced by the underlying Poisson point process satisfy by construction symmetry under reversal $\Omega_\pm \to \Omega_\mp$, which means that in dimension $d = 1$ it will not be possible to introduce anisotropy (direction-dependent) effects for the Markov media sampled by this two-step strategy.

Alternative coloring procedures can be devised also leading to Markov media. In particular, if the cells induced by a Poisson point process are deterministically assigned colors so that each point is a frontier between $\alpha = 0$ and $\alpha = 1$ labels, the resulting binary stochastic media satisfy again the Markov line property, with parameter $\rho_\alpha(x, \Omega_\pm) = \rho(x)/2$ [39].

III. MARKOV MEDIA BASED ON COLORED POISSON TESSELLATIONS

The possibility of extending the Markov media construction to higher dimensions has been an open question for several years. Pielou conjectured that it was possible to have two-dimensional random media whose line transects had a Markov property [25]: this hypothesis was initially questioned by Bartlett [26], until Switzer provided a constructive description of a two-step procedure leading to planar stochastic media with the sought line-Markov property [27]. The existence of a three-dimensional generalization of the Switzer's procedure was later suggested [3,24] and finally explicitly exhibited in recent years building upon d-dimensional Poisson tessellations, which can be sampled by Monte Carlo methods [15,30,32,33].

A Poisson tessellation is a random division of a d-dimensional space into disjoint polyhedral cells such that the distribution of the distance to the next cell boundary for any point and direction across multiple, independent replicas satisfies the line-Markov property [31]. Such tessellation is induced by a Poisson hyperplane process, conceived by Miles in a series of seminal works as a generalization of the standard Poisson point process [40,41]. Using the representation $K = \{\mathbf{r} \in \mathbb{R}^d : \langle \mathbf{n}, \mathbf{r} \rangle = r\}$, where $\mathbf{n}$ is the unit vector normal to the hyperplane and r is the distance of the hyperplane to an arbitrary origin, each hyperplane K is mapped onto a dual point $M = r\mathbf{n}$. An example in dimension $d = 3$ is illustrated in Fig. 3. The duality allows casting the Poisson hyperplane process into a regular Poisson point process in the P-frame $\{r, \mathbf{n}\}$, which can be fully characterized by assigning the intensity function $g(r, \mathbf{n})$, with $g(r < 0, \mathbf{n}) = 0$ by convention.[3] The tessellation density $\rho(\mathbf{r}, \Omega)$, i.e., the mean number of hyperplanes intersecting a differential segment at position $\mathbf{r}$ with direction Ω, is a key quantity physically corresponding to the typical (inverse) spatial scale of the tessellation. Schneider has shown that $\rho(\mathbf{r}, \Omega)$ is related to the intensity function

---

[3]In dimension $d = 3$, the P-frame in spherical coordinates would naturally be r-ϕ-μ, where r is the offset radius, ϕ an azimuthal angle and $\mu = \cos\theta$, with θ a polar angle.
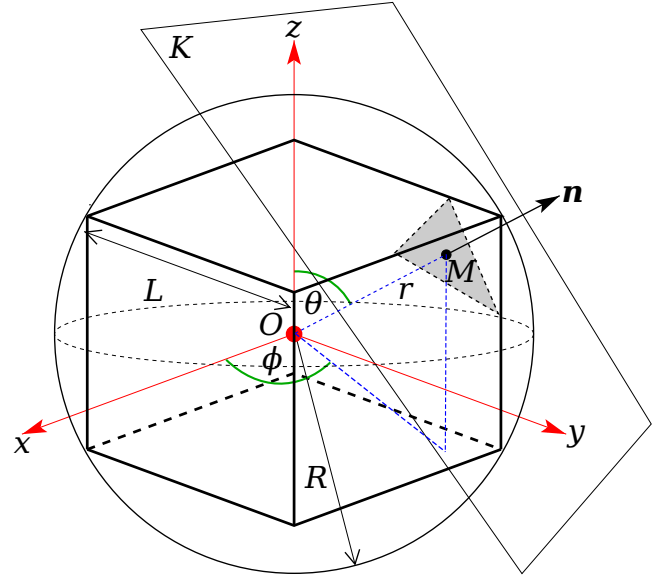

FIG. 3. Sampling of a plane for Poisson tessellation in dimension $d = 3$, inside a cubic domain with side L and centered at O. The random plane $K = \{\mathbf{r} \in \mathbb{R}^3 : \langle \mathbf{n}, \mathbf{r} \rangle = r\}$ is cast into the dual point $M = r\mathbf{n}$, which can be represented in spherical coordinates as r-θ-ϕ. Hyperplanes of the tessellation are sampled by a Poisson point process that generates points M with intensity $g(r, \theta, \phi)$. Scheme adapted from Ref. [33].

$g(r, \mathbf{n})$ by the elegant formula [42]

$$\rho(\mathbf{r}, \Omega) = \int_{S^{d-1}} |\langle \Omega, \mathbf{n} \rangle| g(\langle \mathbf{n}, \mathbf{r} \rangle, \mathbf{n}) \, d\mathbf{n}, \quad (22)$$

where S^{d-1} denotes the surface of the d-dimensional unit sphere, and the integral is restricted to the half-sphere centered on $\mathbf{r}$. The tessellation density is invariant under reflection:

$$\rho(\mathbf{r}, \Omega) = \rho(\mathbf{r}, -\Omega). \quad (23)$$

The underlying Poisson point process ensures a line-Markov property for the resulting Poisson tessellation: an arbitrary line of orientation Ω at position $\mathbf{r}$ will be cut by the hyperplanes of the tessellation into chords whose distribution is nonhomogeneous exponential with parameter $\rho(\mathbf{r}, \Omega)$ [31].

The most general class of Poisson tessellations satisfying Eq. (22) with arbitrary intensity function $g(r, \mathbf{n})$ has been addressed only recently, and very few statistical properties are known exactly [31]. Monte Carlo methods can be used in order to sample the hyperplanes from $g(r, \mathbf{n})$, followed by a computationally expensive enumeration procedure to determine the resulting polyhedral cells. An additional source of difficulty is due to the fact that in order to sample Poisson tessellations with a target density $\rho(\mathbf{r}, \Omega)$ one should solve the integral equation (22) for the intensity function $g(r, \mathbf{n})$, which is a nontrivial task. Special cases of Poisson tessellations, stemming from specific assumptions on $g(r, \mathbf{n})$, may lead to a larger number of analytical results, and simpler sampling procedures. For instance, spatially homogeneous and isotropic tessellations, which are invariant under translation and rotation, correspond to taking a constant $g(r > 0, \mathbf{n}) = \bar{g}$, which
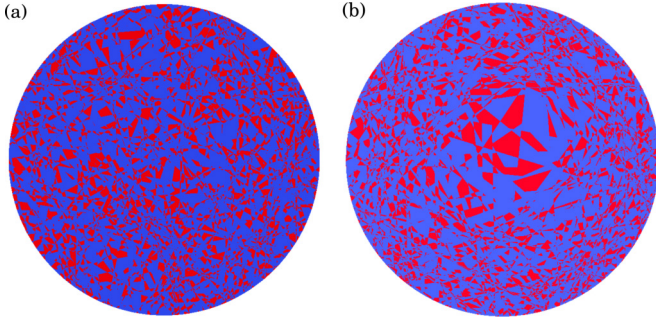
(a)　　　　　　　(b)

FIG. 4. Examples of Markov media produced with the Switzer procedure: two-dimensional cuts of three-dimensional realizations restricted to a spherical domain with radius $R = 10$ and $p_{\rm red} = 0.3$. (a) Spatially homogeneous case, with $\rho = 5$. (b) Spatially heterogeneous case, with radial intensity $g(r) = 5[1/4 + (3/4)u(r - 3)]$, $u(r)$ being the Heaviside step function.

yields a constant density

$$\rho(\mathbf{r}, \boldsymbol{\Omega}) = \bar{\rho} = \frac{1}{2}\bar{g} \int_{S^{d-1}} |\langle \boldsymbol{\Omega}, \mathbf{n} \rangle| d\mathbf{n} = \bar{g}\kappa_{d-1}, \quad (24)$$

$\bar{g}$ being a spatial scale factor and κ_d the volume of the d-dimensional unit sphere [31]. This class of tessellations has been thoroughly investigated, mainly thanks to the pioneering work by Miles [40,41]; yet only the low-order moments of some statistical properties have been computed, and most of their distributions are still unknown [31]. Invariance under rotation can be relaxed by taking

$$g(r, \mathbf{n}) = \bar{g}H(\mathbf{n}), \quad (25)$$

where $H(\mathbf{n})$ is the angular distribution of the hyperplanes, with normalization $\int_{S_+^{d-1}} H(\mathbf{n}) d\mathbf{n} = 1$ on the positive half-sphere S_+^{d-1}. This leads to the class of nonisotropic (but spatially homogeneous) Poisson tessellations with direction-dependent density

$$\rho(\mathbf{r}, \boldsymbol{\Omega}) = \rho(\boldsymbol{\Omega}) = \bar{\rho} \int_{S_+^{d-1}} |\langle \boldsymbol{\Omega}, \mathbf{n} \rangle| H(\mathbf{n}) \, d\mathbf{n}, \quad (26)$$

whose statistical properties are much more involved than in the isotropic case and seldom known explicitly [31]. It is worth mentioning that the superposition of two Poisson tessellations is again a Poisson tessellation, whose density is the sum of the respective densities [31]: this property can be usefully applied in order to impose very broad shapes of spatial gradients in $\rho(\mathbf{r}, \boldsymbol{\Omega})$.

Markov media are finally obtained from Poisson tessellations using the Switzer's "coloring" procedure, i.e., assigning each cell of the tessellation a color α with independent probability p_α, which leads to general d-dimensional N-ary material mixtures. For illustration, some examples of binary Markov media are displayed in Fig. 4. It can be shown that material chunks with label α have colored chord lengths obeying a nonhomogeneous exponential distribution as in Eq. (1), with parameter

$$\rho_\alpha(\mathbf{r}, \boldsymbol{\Omega}) = (1 - p_\alpha)\rho(\mathbf{r}, \boldsymbol{\Omega}). \quad (27)$$

The alternative "deterministic" binary coloring discussed in Sec. II B trivially generalizes to d-dimensional Poisson
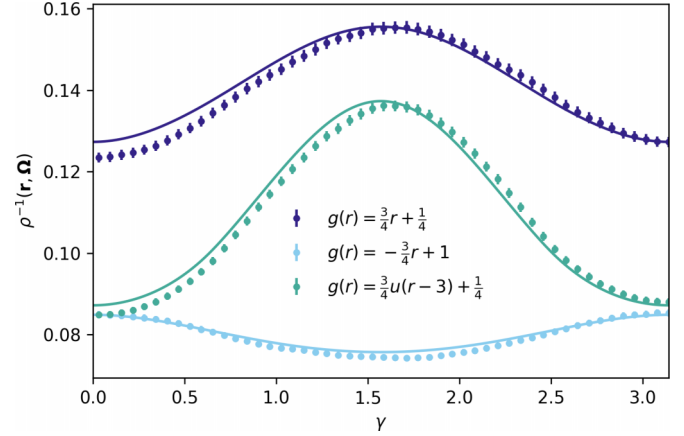

FIG. 5. Comparison of the Monte Carlo estimated average chord length (symbols) against the values of $1/\rho(\mathbf{r}, \boldsymbol{\Omega})$ obtained from Eq. 22 (solid line) at point $\mathbf{r} = (5, 0, 0)$ for three-dimensional heterogeneous Poisson tessellations with radial intensity $g(r, \mathbf{n}) = 5g(r)$, restricted to a sphere of radius $R = 10$. Here $u(r)$ denotes the Heaviside step function. The angle γ represents the polar deflection from the radial direction. Error bars correspond to one σ statistical uncertainty.

tessellations: each hypersurface of the cells will be a discontinuity between colors, and the line-Markov property still holds true, with $\rho_\alpha(\mathbf{r}, \boldsymbol{\Omega}) = \rho(\mathbf{r}, \boldsymbol{\Omega})/2$.

A Monte Carlo code, named CASTOR, has been developed at CEA for the purpose of sampling d-dimensional Markov media resulting from the Switzer two-step approach: in recent years, it has been successfully applied in the context of particle transport problems, for homogeneous and isotropic configurations [13,15,16], anisotropic configurations [14] and configurations with spatial gradients [33].

For the purpose of illustration, we have examined the chord length distribution for a few relevant examples of spatially heterogeneous Switzer media. Since the colored chord lengths are simply related to the uncolored chord lengths by Eq. (27), it suffices to probe the underlying Poisson tessellation by verifying Eq. 22. For our numerical tests, we have sampled heterogeneous Poisson tessellations having symmetry with respect to rotations around the origin [i.e., $g(\mathbf{r}, \mathbf{n}) = g(r)$], so that the angular dependence of the tessellation density is limited to a polar deflection angle γ from the radial direction. We have compared the Monte Carlo estimator of the mean chord length at a point $\mathbf{r}$ in a specific direction $\boldsymbol{\Omega}$ to the quantity $1/\rho(\mathbf{r}, \boldsymbol{\Omega})$ from Eq. (22). The large computational cost required to construct three-dimensional realizations has conditioned the choice of this estimator, which is admittedly rather crude; hence, Monte Carlo estimates are expected to agree with the theoretical formula as long as the spatial gradient is much smaller than the mean chord length. Simulation results are displayed in Fig. 5 and show that, although the agreement is rather good, this hypothesis is only partially satisfied.

Although the spatial structure of Markov media obtained through the Switzer procedure is rather rich, and accounts in principle for arbitrary gradients and anisotropy in the spatial scale $\rho(\mathbf{r}, \boldsymbol{\Omega})$ via the flexibility of the underlying Poisson tessellations, the requirement of spatially constant p_α implies that no gradient can be imposed on the material phases: this is

basically the same restriction as in the one-dimensional case discussed in Sec. II B. For the same reason, the possibility of sampling Markov media displaying complex conditional transitions between phases in N-ary material mixtures is also forbidden in this construction [43]. A further limitation of this class of Markov media is the difficulty in imposing strong spatial gradients in $\rho(\mathbf{r}, \mathbf{\Omega})$, due to the combined action of the smoothing effect of the integral in Eq. (22) and the long-distance correlations induced by the Poisson hyperplane process [33].

IV. MARKOV MEDIA BASED ON ARAK'S MODEL

One-dimensional random media have a peculiar feature, in that material chords coincide with material regions: Markov line transects imply a spatial Markov property. This is clearly not the case for higher-dimensional random media: in the context of particle transport, for historical reasons the term "Markov geometries" is used for media having Markov line transects, but not being necessarily Markov in the spatial sense. Loosely speaking, random media in a bounded convex region V are endowed with a spatial Markov property if the interior coloring of a region $V' \subseteq V$ is conditionally independent of the exterior coloring, given the knowledge of the color process on the boundary $\partial V'$, i.e., information about both the colors on $\partial V'$ and the coordinates of the hypersurfaces defining the frontiers between the colors [39].

In this respect, the Switzer procedure based on independently colored Poisson tessellations leads to media that are not spatially Markov: due to the long-range correlations induced by the underlying Poisson hyperplane process, some of the hyperplanes that cross the boundary $\partial V'$ of a region $V' \subseteq V$ of the tessellation do not induce an interface between colors on $\partial V'$, while inducing (with probability one) an interface between colors outside V' [39]. The information content on $\partial V'$ is thus not equivalent to that on the exterior of V'. Conversely, the deterministic binary coloring is spatially Markov, due to the fact that all the hypersurfaces of the cells are visible, being by construction interfaces between colors.

An intriguing question is thus whether other, less restrictive d-dimensional stochastic media having the spatial Markov property exist. A class of two-dimensional random media having polygonal realizations and endowed with such property has been introduced by Arak [34] and considerably extended by Arak, Surgailis, and Clifford [35–37]. We denote by "coloring" a function ω mapping a bounded region V of the plane into a finite space of discrete labels (i.e., colors). Consider a finite set $\ell = \{l_1, l_1, \ldots, l_n\}$ of lines intersecting V, and let Ω_V^ℓ be the set of all colorings of V such that each line $l_i \in \ell$ has a segment $[l_i]$ of strictly positive length where ω is discontinuous, with the constraint that the set of discontinuities of ω is $\bigcup_{i=1}^n [l_i]$. Note that each line can contribute only a single segment: two edges of a valid coloring will not be colinear almost surely. For an illustration, see Fig. 6. The set of all such polygonal colorings is denoted by $\Omega_V = \bigcup_\ell \Omega_V^\ell$. A polygonal mosaic is introduced by assigning the probability measure

$$\mathcal{P}_V(A) = \left\langle \sum_{\omega \in \Omega_V^\ell \cap A} \frac{e^{-F(\omega)}}{\mathcal{Z}_V} \right\rangle \qquad (28)$$
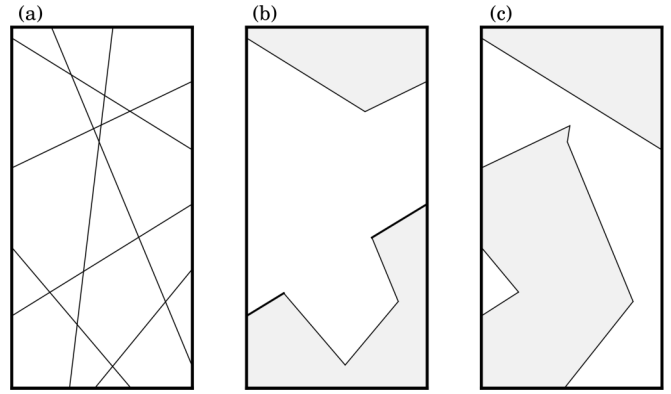

FIG. 6. Examples of two-dimensional colorings with polygonal realizations [44]. (a) Set of lines intersecting a rectangular domain V. (b) Invalid coloring based on the set of lines at the left: a single line (marked in bold) contributes to two edges. (c) Valid coloring based on the same set of lines: here each line contributes to a single edge inside V.

to coloring events $A \subset \Omega_V$. The expectation over ℓ in Eq. (28) is taken with respect to the Poisson line process on V, and $F(\omega)$ is a potential function mapping the set Ω_V of possible coloring into $\mathbb{R} \cup \{\infty\}$. The quantity $\mathcal{Z}_V$ is the normalization factor of $\mathcal{P}_V(A)$, i.e., the partition function of the probability measure on Ω_V. A sufficient condition for polygonal mosaics to have the spatial Markov property is that the potential $F(\omega)$ is additive, i.e., the value of F applied to the entire region V equals the sum of the potentials applied to the partitions of V [35]. Examples of additive potentials are, e.g., the total length of the discontinuity boundary between colors, the total area of a given color, and so on. Arak and Surgailis have exhibited a very broad family of additive potentials F for which the resulting Markov polygonal mosaics are endowed with the following features: they are "consistent," i.e., the mosaic of the region V' is equal in distribution to the restriction to V' of the mosaic of the region V, for $V' \subseteq V$; the partition function $\mathcal{Z}_V$ is finite and has an explicit expression; and one-dimensional transects have the line-Markov property [35,36].

Clifford and Middleton have proposed a Monte Carlo sampling strategy that allows generating a collection of Markov polygonal mosaics [39,45]: the underlying idea is to build a Markov chain on the set Ω_V of possible polygonal colorings, based on a "skeleton" provided by a Poisson line process, and to accept or reject the proposed changes in the coloring via a Metropolis-Hastings algorithm in such a way that the distribution of the coloring converges to Eq. (28) at equilibrium. Practical sampling of Arak geometries was proved to be feasible using a clever scheme that eliminates the need for the (extremely expensive) combinatorial enumeration of the possible colorings [46]. Further theoretical results [47] and the growth in available computer power have fostered the development of conceptually and computationally easier algorithms [48–52], which have been successfully used, e.g., in the field of image analysis.

A. Particle representation of the Arak model

A peculiar feature of the Markov polygonal mosaics is that they can be alternatively represented in terms of a Markov
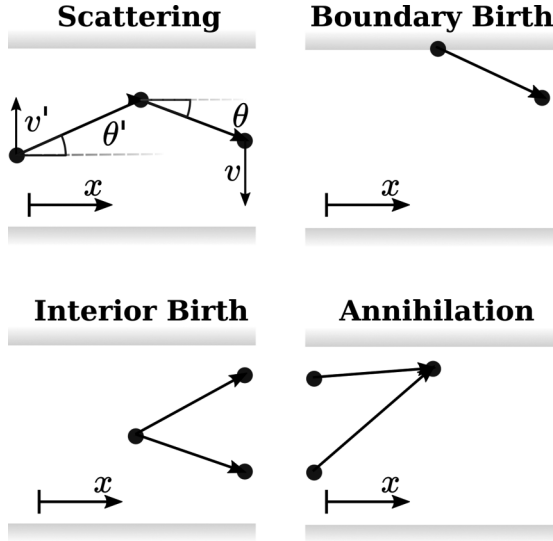
FIG. 7. Illustration of the four main types of events in the dynamics of the particle system resulting in Arak media. Leakage through the boundaries is not shown. The notation used for velocity and angles is given for the case of scattering. The angle θ is positive in counterclockwise direction.

process of particles. It turns out that a two-dimensional random geometry having the same distribution as the Arak model described above can be constructed by simulating the stochastic evolution of a system of interacting particles, placed on a line segment and evolving in time [35]: one of the spatial axes (usually x) becomes the "time" variable of the process, whereas the other axis (say, y) denotes the spatial coordinate of the particles. Following the simulation of the system of particles (whose stochastic rules are detailed in the following) on some rectangular window V spanning $x \in [0, L_x]$ and $y \in [0, L_y]$, the free flights of the particles moving at constant speed between subsequent "collision events" generate the set $\bigcup_n \{x_n, y_n(x)\}$ of the edges of the random media. The colors above and below each particle trajectory are assumed to be always different, so that the paths of the particles define the "color discontinuities" of the resulting random medium in the x, y coordinates. Furthermore, storing the color information in each edge is sufficient to later determine the color at each point in the geometry. General N-ary mixtures can be represented in that fashion; in the simpler case of binary mixtures, it is sufficient to note that the color systematically changes when crossing a path traced by a particle.

Clearly, the key question is the relationship between the types and rates of events that can happen to the particles and the properties of the resulting two-dimensional geometry. Fortunately, this question has been answered in the case of homogeneous settings in the foundational papers by Arak and Surgailis [35,36]. Here we will summarize their findings for the case of homogeneous and isotropic binary Markov media constructed on a rectangular window V. We restrict our discussion to the following set of events for the Arak particle process, summarized in Fig. 7. A random number of particles is sampled at the initial condition at $x = 0$, as detailed below. Furthermore, particles can be created in two

ways: either a particle enters from outside the geometry and is spawned at the top or bottom boundary, or a pair of particles is created in the interior of V. Once created, particles move in space at constant velocity v, until an event occurs. The quantity v, which is related to the dynamics of the stochastic process, can be expressed as $v = \tan \theta$ in terms of the angle $\theta \in [-\pi/2, \pi/2]$ of the particle path with respect to the x axis, which is a geometrical property.[4] Particles can scatter, whereupon the particle velocity randomly changes. Finally, particles can be removed by two deterministic events: they can either leak through the top or bottom boundary of V, or two particles may annihilate each other if their trajectories collide in the interior of V. In the original model proposed by Arak and Surgailis, a much more general class of stochastic processes was considered, with additional events leading in turn to more complex polygonal shapes in the resulting random media [35,36], but for clarity we will focus on a simpler, yet nontrivial version.

To fully define the dynamics of the system of interacting particles, the following distributions are required: the distribution of the initial state (position and velocity) of the system at time $x = 0$; the probability that a particle will scatter in an infinitesimal time interval dx around x, as well as the distribution of the outgoing velocity; the probability that a particle will be spawned at the top or bottom boundary in an infinitesimal time interval dx around x and its velocity distribution; and finally the probability that a pair of particles will be created at $dxdy$ around coordinates x, y and their velocity distributions. In addition, it is necessary to specify the density parameter ρ and the color fraction p_α (with $\alpha \in \{0, 1\}$).

The initial state of the particle system at $x = 0$ is determined as follows: a collection of starting positions is sampled from sweeping a Markov process on the line segment from $y = 0$ to $y = L_y$. The initial color α at $y = 0$ is sampled randomly using p_α, and the rates of the process are assigned as $\rho_\alpha = \rho(1 - p_\alpha)$, depending on the color and on the spatial scale. Each color discontinuity point on the segment becomes a starting particle for the Arak model. The corresponding angular distribution for the first flight paths reads

$$a_s(\theta) = \frac{\cos(\theta)}{2}, \tag{29}$$

from which the velocity v of the source particles can be promptly sampled.

Somewhat surprisingly, the scattering rates of the Arak model are color-sensitive, and also depend on the colors immediately above and below a particle. A particle traveling with velocity $v' = \tan \theta'$ and having phase β above and $\alpha \neq \beta$ below will undergo upward scattering ($v \geqslant v'$) with rate $2q_\beta\sqrt{1 + u'^2}$, and conversely downward scattering ($v \leqslant v'$) with rate $2q_\alpha\sqrt{1 + v'^2}$. For a given color α, the rate q_α is defined as $q_\alpha = (1/2)\rho_\alpha$. Qualitatively speaking, the particles tend to be deflected in the direction of a phase with higher ρ_α. The factor $\sqrt{1 + v'^2}$ accounts for the projection on the time

----

[4]Our convention on θ is slightly different from the one in the original papers [35,36].

TABLE I. Arak model: rates of different events in dx, together with the associated velocity distributions. We assume that the space around the particle is occupied by phase α above, and by phase β below (with $\alpha \neq \beta$).

Event	Rate	Velocity distribution
Top boundary birth	q_α	$v^-(v, 0)$
Low boundary birth	q_β	$v^+(v, 0)$
Pair birth	$\pi q_0 q_1 dy$	$v(v_2, \tan(\theta_1))$ and $\theta_1 \sim \mathcal{U}(-\frac{\pi}{2}, \frac{\pi}{2})$
Scattering +	$2q_\alpha \sqrt{1 + u^2}$	$v^+(v, v')$
Scattering −	$2q_\beta \sqrt{1 + u^2}$	$v^-(v, v')$

axis. The velocity distribution for upward scattering is

$$v^+(v, v') \propto \begin{cases} v(v, v'), & \text{if } v \geqslant v' \\ 0, & \text{if } v < v', \end{cases} \quad (30)$$

the case of downward scattering $v^-(v, v')$ being similarly defined, with

$$v(v, v') = \frac{|\sin(\tan^{-1} v - \tan^{-1} v')|}{2(1 + v^2)}. \quad (31)$$

The origin of Eq. (31) is the following. Given a particle path with orientation θ', the orientation θ of the path after the scattering event is chosen so that $\theta - \theta'$ has the same distribution as the angle between the lines of a Poisson line process, which is key for the resulting geometry induced by the Arak model to display a Markov property. This implies the angular distribution [40]

$$a(\theta, \theta') = \frac{|\sin(\theta - \theta')|}{2}, \quad (32)$$

whence, using the definition of v, v' in terms of θ, θ', and the transformation of variables

$$v(v, v') = a(\theta, \theta') \cos^2 \theta \quad (33)$$

we recover Eq. (31) for the velocity distribution. Observe that $a_s(\theta) = a(\theta, \pi/2)$, which means that the angular distribution of the source particles can be formally assimilated to a scattering event where the incident particle direction is aligned along the y axis (i.e., the velocity $v' \to \infty$). The sampling of v, given the incident velocity v', is achieved quite simply using the inversion theorem:

$$v = \tan\left[\cos^{-1}(1 - 2\xi) + \tan^{-1} v'\right], \quad (34)$$

where ξ is a uniform random variable in $[0, 1)$.

The birth events at the top ($y = L_y$) and bottom ($y = 0$) boundaries are similar to scattering events. A particle having phase α below (resp. above) will be produced at the top (resp. bottom) boundary with rate q_α, with associated downward (resp. upward) velocity distribution $v^-(v, 0)$ [resp. $v^+(v, 0)$]. Since the boundaries are parallel to the time axis, the correction factor $\sqrt{1 + v'^2}$ does not appear in the rates. Furthermore, the rates are halved with respect to scattering, because births contribute only to the half of the intersections of the particle paths with the boundaries, the other half being due to particles reaching the top or bottom boundary of the rectangular window V and being removed.

The rate of the spontaneous births of pair of particles in the interior of V is color-independent: these events are defined by a two-dimensional Poisson point process on V with intensity

$\pi q_\alpha q_\beta$. The velocity of the pair of particles is determined by first sampling a uniform angle $\theta \in [-\pi/2, \pi/2]$ and obtaining $v_1 = \tan \theta$ for the first particle, and then sampling v_2 from $v(v_2, v_1)$ for the second particle. The justification for this choice is again related to the properties of the resulting geometry induced by the particle paths and its intimate connection with Poisson line processes.

The events of the Arak model are summarized in Table I. The two-dimensional coloring induced by the edges defined by such interacting particle process satisfies a spatial Markov property. Furthermore, line transects of arbitrary orientation will display a line-Markov property, with chord length density $\rho_\alpha = \rho(1 - p_\alpha)$ [35,36]. Similarly to Markov media constructed using the Switzer procedure, the properties of the colored chords of Arak media depend on a spatial scale factor ρ and on the color probability p_α, which is convenient in view of comparing these two Markov media. For illustration, a representative evolution of a particle system and the resulting
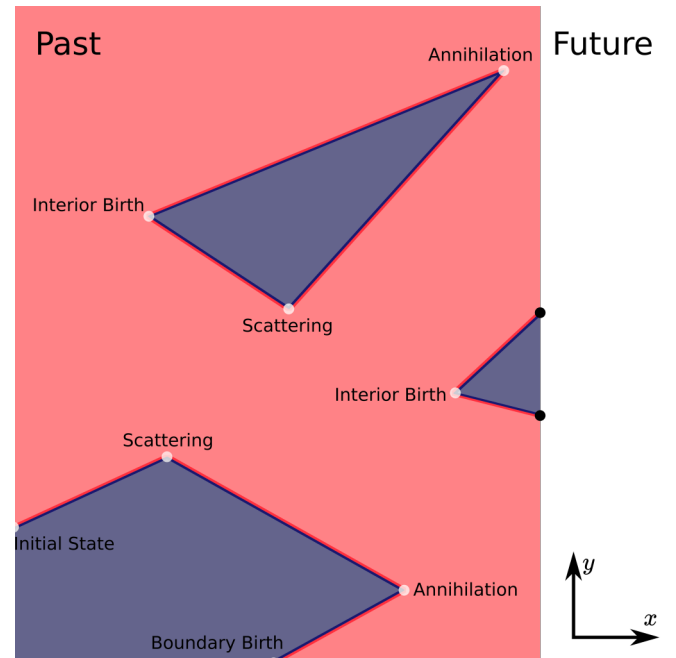

FIG. 8. An example of the evolution of the Arak particle system on a square window. Each particle traces an edge which is assigned a color on both sides (note the two colors composing an edge on the diagram). The color of regions enclosed by edges is implicitly determined by color on its boundary. Each event is annotated with its type and marked by a white dot. Black dots represent particles present in the configuration at a particular instant.

geometry are shown in Fig. 8, with each event annotated with the corresponding type. Note that the color information is contained within double-colored edges. The color of the cells is implicitly defined by the color of their boundary.

B. Implementation of Arak particle construction

The main advantage of the particle representation of the Arak model is that it is more efficient to simulate than the Markov chain Monte Carlo (MCMC) schemes based on the potential representation, which typically require a large number of iterations to converge. Furthermore, the expression for the potential $F(\omega)$ becomes extremely complex for the case $p_\alpha \neq 1/2$: it involves terms related to the number of closed "loops" formed by edges around a chunk of a given color [as shown in the last term of Eq. (3.3) in [36]].

In order to sample realizations of Arak media for numerical investigations, we have developed a C++ code by the name of POLLUX. The main idea in the simulation of the evolving system of particles is to store all the events in a priority queue and process each of them sequentially, for increasing time. Whenever a particle is created or undergoes scattering, an event descriptor for its next collision with another particle of the system is stored in the event queue. The same is done for the sampled time of its next scattering event. The main challenge in the simulation is the fact that some event descriptors in a queue may become invalid, since a particle involved in an interaction may undergo scatter or be annihilated at an earlier time. This raises the question of how one would keep the event queue up to date with the current state of the system. The answer to this problem is to supply an "event validation" mechanism. Basically, each free-flight edge of the geometry may be assigned a unique identifier, which is stored in the event descriptor of its interaction (the scattering descriptor stores a single identifier, whereas an annihilation descriptor stores two). In addition, unique identifiers of all edges present in the current state of the system are kept in a set. Thus, once an event is removed from a queue, the identifiers of its participants can be checked against the set. If they are all present, the time must be advanced and the event processed. If any is missing, the event is invalid and needs to be ignored.

Since the event rates are color-dependent, special care must be taken so to ensure that the system of simulated particles is consistent: the color of the region between neighboring particles must be the same as for the "top" and "bottom" particle. To construct the geometry, after each event a free-flight segment is saved together with the colors immediately above and below it. Thus, the final geometry is represented as a collection of colored edges, which mark the boundaries between different faces. In contrast to colored Poisson tessellations, the cells of Arak media are not explicitly represented. To determine which phase occupies a given point, it is necessary to emit a ray in any direction and to find its nearest intersection with an edge, from which the color can be read. To accelerate the search for the closest intersection, a Cartesian search mesh is used to limit the number of the edges that need to be checked. This strategy, while not being the most efficient way to represent the geometry, has proven sufficient to perform particle transport calculations and geometry visualization of moderately large (or dense) geometries.

(a) $p_{red} = p_{blue} = 0.5$

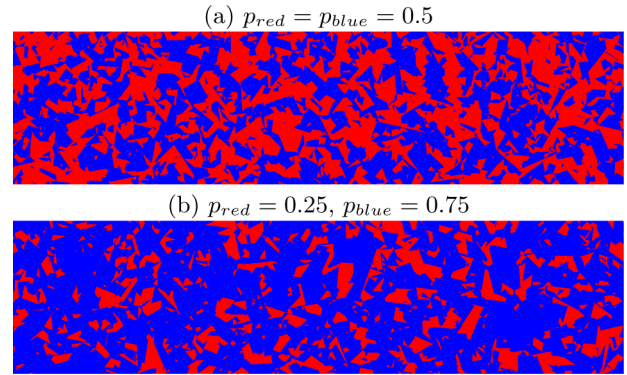(b) $p_{red} = 0.25$, $p_{blue} = 0.75$

FIG. 9. Examples of realizations of spatially homogeneous Arak media for two color fractions and $\rho = 30$. Note that only two edges can meet at a point (V-shaped nodes) and there are no colinear edges, contrary to the Markov media sampled with the Switzer procedure shown in Fig. 4.

To allow easier experimentation with different types of particle dynamics, POLLUX separates the code which performs the particle evolution and geometry construction from the code which samples the events and velocity distributions, which is hidden behind an abstract interface. This approach significantly reduces the effort required to introduce new kinds of events in the stochastic process. Some examples of realizations of Arak media are shown in Fig. 9. At present, POLLUX is limited to work with events leading to geometries whose lines are connected by V-shaped nodes only. However, the support of Y- and X-shaped nodes (which can be mixed in different proportions together with V-shaped nodes) will be introduced in a near future.

In order to verify our implementation, we have used the same strategy as in [46], relying on analytical results for the expected number of points and edges in a geometry with $p_\alpha = 1/2$: numerical tests have shown very good agreement, as summarized in Table II. For the case of $p_\alpha \neq 1/2$, analogous analytical formulas are unavailable in the literature, so we have focused instead on the chord length distribution and the volume fractions.

TABLE II. Monte Carlo verification of the Arak construction on a unit square based on expected number of interior points and edges, whose expressions are given in [46], for the case $p_0 = 1/2$. For each ρ, 1.0×10^7 samples were drawn.

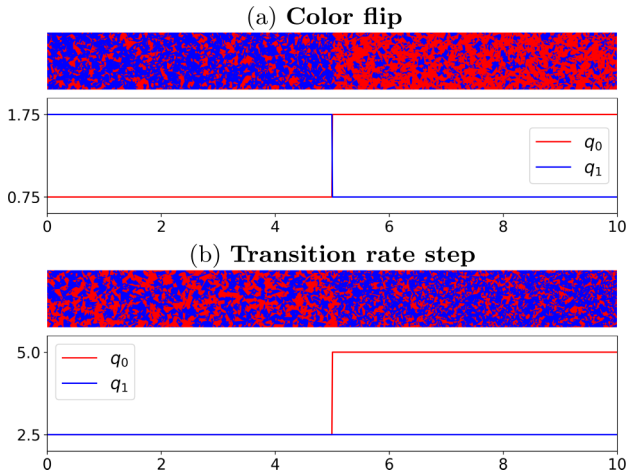| ρ	Expected number of points	Monte Carlo
0.01	7.854×10^{-5}	$7.370(272) \times 10^{-5}$
0.1	7.854×10^{-3}	$7.822(29) \times 10^{-3}$
1	7.854×10^{-1}	$7.851(3) \times 10^{-01}$
10	7.854×10^{1}	$7.854(0) \times 10^{1}$
ρ	Expected number of edges	Monte Carlo
0.01	1.0079×10^{-02}	$1.0096(2) \times 10^{-02}$
0.1	1.0785×10^{-01}	$1.0797(2) \times 10^{-01}$
1	1.7854	$1.7851(3)$
10	8.8540×10^{1}	$8.8542(4) \times 10^{1}$

FIG. 10. Examples of realizations for the spatially heterogeneous Arak media investigated in Sec. IV C, together with the corresponding transition rates $q_\alpha(x)$. For visualization, the magnitude of the rates was increased by a factor of $\times 10$ in the color flip case and $\times 4$ in the step case in order to emphasise the gradient in the displayed realizations.

C. Heterogeneous Arak model

The logic of the particle construction for the Arak model is significantly different from the one used in the construction of Markov media using Poisson tessellations: a strong resemblance with the "sweeping" construction of Markov media on the line is apparent. Based on this analogy, it seems reasonable to introduce one-dimensional gradients in the spatial properties of Arak media in a fashion similar to the heterogeneous one-dimensional Markov media, i.e., by assuming that the particle dynamics is time-dependent. This can be achieved by making the Arak transition rates $q_\alpha(x)$ functions of "time" x, which in turn implies that all event rates in Table I become also time-dependent. While it can be reasonably argued that the resulting stochastic process is still Markov, to the best of our knowledge this *ad hoc* generalization of the Arak model lacks a fully developed theoretical support, since most of the existing literature discusses exclusively the case of time-homogeneous Arak dynamics. In this paper we will not attempt to formulate rigorous proofs for the statistical properties of heterogeneous Arak media, but instead propose semi-formal arguments carefully supported by Monte Carlo simulations.

To enable sampling particle events from a nonstationary dynamics in POLLUX, we implemented a rejection scheme similar to the delta-tracking method [53]. The time-dependent events of the Arak dynamics are sampled based on the time-independent $q_\alpha^{\max}$ rate, and accepted with probability $q_\alpha(x)/q_\alpha^{\max}$, where $q_\alpha^{\max}$ is a precomputed upper bound on the values of $q_\alpha(x)$. The standard Lewis's thinning method [54] is employed to sample particle birth sites from a nonstationary two-dimensional Poisson point process. For illustration, some examples of realizations corresponding to a step change in color fractions and a step change in single transition rate are shown in Fig. 10. Theorem 8.1 of [35] states that the geometry generated by the Arak particle dynamics has the spatial Markov property provided that the associated potential

$F(\omega)$ is additive (and the partition function $\mathcal{Z}_V$ is finite). The additivity of the potential function of the heterogeneous Arak model follows from $F(\omega)$ behaving as in the homogeneous case for sufficiently small regions $dx\,dy$. The line-Markov property has been assessed by resorting to Monte Carlo, via a two-step verification process: we have first generated an ensemble of realizations of Arak media, from which the chord length densities $\rho_\alpha(\mathbf{r}, \mathbf{\Omega})$ have been estimated; then, a new, independent ensemble of realizations has been sampled and used to estimate the colored chord length distribution. The histogram of the chord length distribution is finally compared to the nonhomogeneous exponential distribution in Eq. (1) having the inferred transition rates.

The chord length densities $\rho_\alpha(\mathbf{r}, \mathbf{\Omega})$ of the resulting nonhomogeneous Arak media were estimated as follows: for each realization, a test segment of length 0.001 was placed at point $\mathbf{r}$ in direction $\mathbf{\Omega}$, the color at $\mathbf{r}$ was found and the next intersection in direction $\mathbf{\Omega}$ was determined. Thus, by recording whether this transition took place within the length of the test segment, it was possible to measure the probability of a color change, which yields the chord length densities under the approximation that they are constant over the length of the test segment. We have investigated a few relevant configurations, with spatial gradients based on the ones used previously for the one-dimensional heterogeneous Markov media on the line. The Arak transition rates $q_\alpha(x)$ were chosen to match the ones imposed in the one-dimensional cases illustrated in Fig. 2. Furthermore, the location of test points were the same for both models. For the chord length densities, 1.0×10^8 independent replicas were sampled. Chord length distributions in the forward and backwards directions parallel to the x axis were measured, based on additional 2×10^7 independent replicas.

The chord length densities as well as the comparison between measured and theoretical chord length distributions are displayed in Fig. 11 for directions aligned with the x axis. Figure 12 displays the comparison of the chord length distributions against theoretical curves for directions aligned with the y axis and with $\pi/4$ deflection direction. Clearly, there is a statistically significant agreement between measured and theoretical chord length distributions, which is a strong evidence that the line-Markov property is preserved in the case of spatially heterogeneous Arak geometries. As far as we are aware, this is the first time two-dimensional heterogeneous Markov media with gradients in the color fractions $p_\alpha(\mathbf{r})$ are explicitly exhibited.

As expected, the observed chord length densities $\rho_\alpha(\mathbf{r}, \mathbf{\Omega}) = \rho_\alpha(x)$ projected on the positive direction of the x axis do not reproduce the Arak transition rates $q_\alpha(x)$ exactly. There is a noticeable lag in the measured chord length densities, which may be attributed to the fact that the observed $\rho_\alpha(x)$ in the Arak media depend not only on the rates $q_\alpha(x)$ of the Markov process used to generate the geometry, as it was the case in one-dimensional Markov media, but also on the current state of the particle system. Basically, after each step change in the dynamics, particles require a relaxation time to reach a new equilibrium state. The "lag" of the $\rho_\alpha(x)$ is key to predicting the statistical properties of nonhomogeneous media: for this purpose, at present we rely on the stochastic measurement of the chord length densities; future work will be devoted to developing theoretical tools for the analysis of
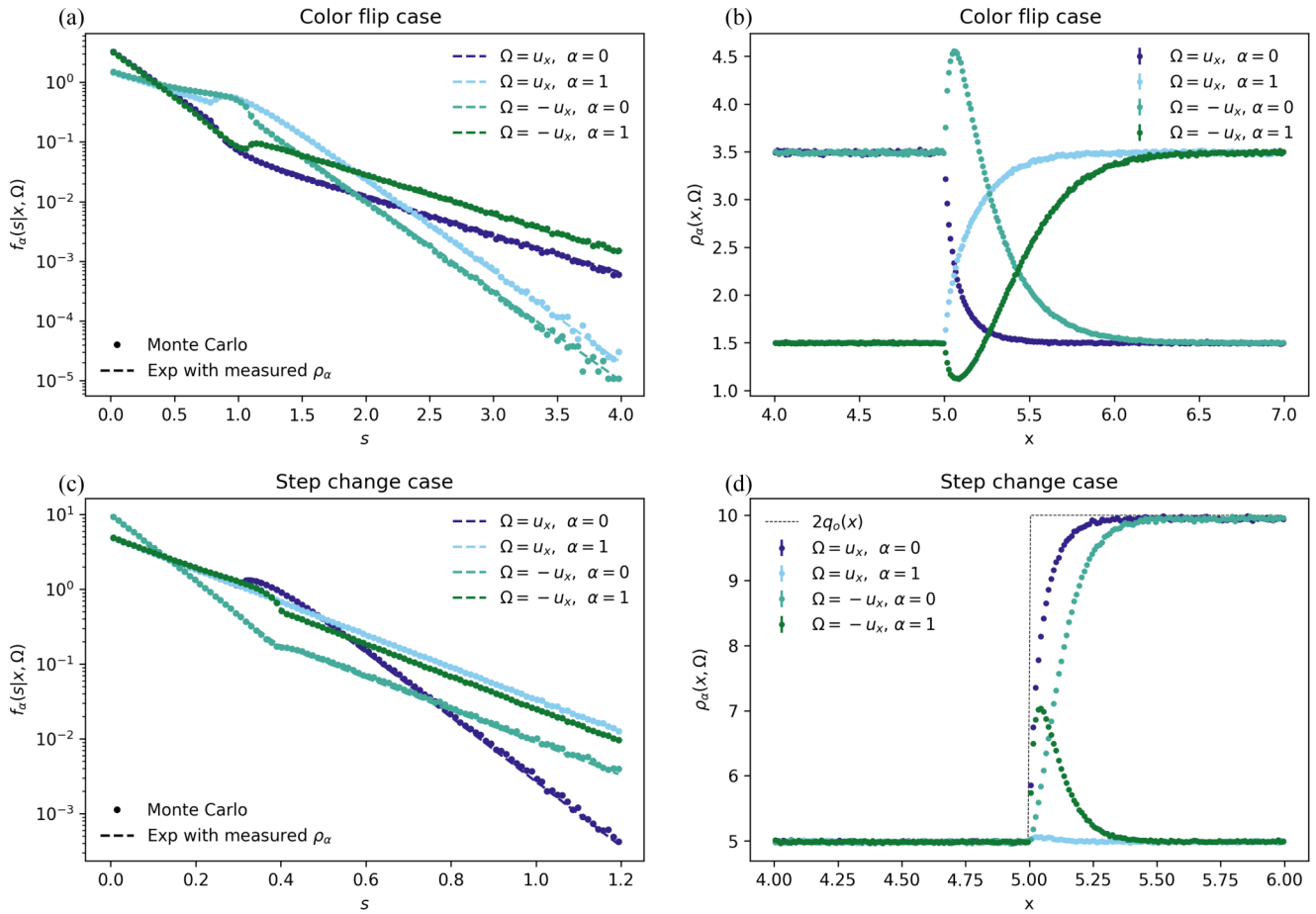
FIG. 11. Statistical properties of Arak media with spatial gradients. (a, c) Comparison of the Monte Carlo histogram of the chord length distribution against the formula assuming that the distribution given by Eq. (1). Here u_x is used to denote the unit vector along the x axis. The dashed line representing the postulated distribution has a statistically significant agreement with respect to Monte Carlo sampled values. [(b), (d)] Estimated measured transition rates. Error bars (barely visible) represent one σ statistical uncertainty. Chord length and transition rates were estimated on independent sets of realizations. For the step change case, the shape of the Arak transition rate $2q_0(x)$ is shown to emphasize that the transition rate behaves similarly as in one-dimensional Markov media on the line.
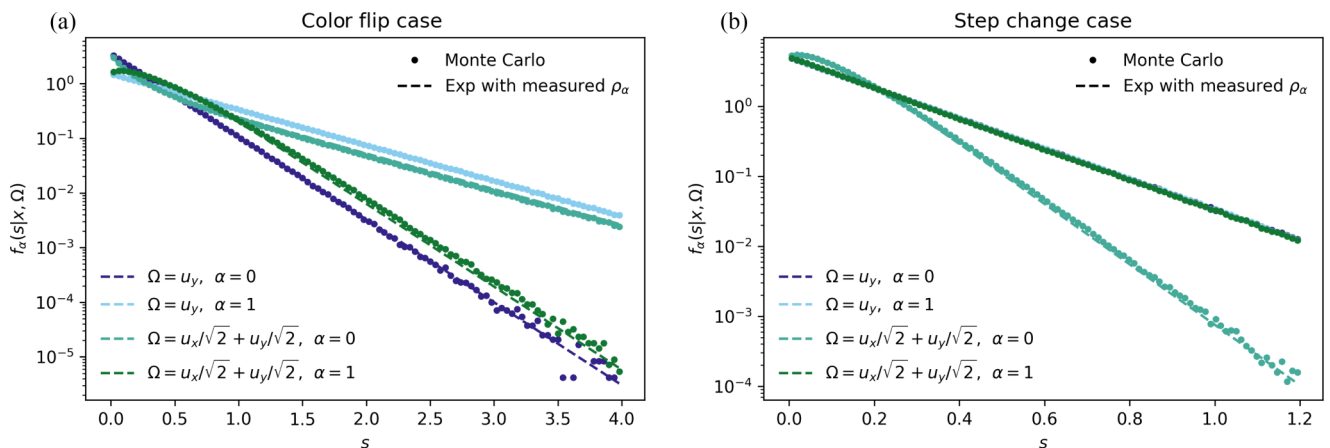

FIG. 12. Comparison of the Monte Carlo histogram of the chord length distribution against the formula assuming the distribution given by Eq. (1) for directions not aligned with the x axis. The same statistically significant agreement as in Fig. 10 can be observed. The test point for all cases was placed at $x = 5$. Note that in (b) three of the cases yield the same homogeneous exponential chord length distribution (displayed as a straight line).

this behavior. The same "lag" phenomenon also accounts for the fact that the discontinuities observed in the chord length distributions for one-dimensional Markov media are absent from the those measured in Arak media. Notwithstanding these discrepancies, the overall qualitative features of $\rho_\alpha(x)$ for one-dimensional and Arak media are very similar.

V. COMPARISON OF SWITZER AND ARAK MODELS FOR PARTICLE TRANSPORT PROBLEMS

In this section we examine the impact of the different Markov media models on particle transport problems, which is the primary motivation for this work. Since particle histories are composed of a series of successive exponential flights in between collisions with direction reorientation, a widely adopted assumption is that transport in random media is primarily affected by the colored chord length distribution (and in particular the average chord length) [2]. We would like then to assess to which extent Switzer and Arak media sharing the same chord length distribution (but generally having different higher-order spatial correlations) may show discrepancies in transport-related observables, such as the ensemble-averaged flux. For this purpose, we have selected a simple configuration for particle transmission, adapted from the higher-dimensional version of the celebrated Adams-Larsen-Pomraning benchmark [15]: the Boltzmann equation for single-speed transport was solved by Monte Carlo simulation in a cube with a side length of $L = 10$ filled with spatially homogeneous realizations of the random media. The random media are binary mixtures of a pure absorbing material for phase $\alpha = 0$ (with cross section $\Sigma_0 = 10/99$) and pure isotropically scattering material for phase $\alpha = 1$ (with cross section $\Sigma_1 = 100/11$). Since the Arak model is inherently two-dimensional, the realizations were extruded along the z axis; for a fair comparison, for the Switzer geometries we have also sampled two-dimensional configurations and extruded them along the z axis. An isotropic source has been placed at the side $x = -5$ of the box, and vacuum boundary conditions have been imposed on the opposite face at $x = 5$; reflective boundary conditions were imposed on the y and z axes.

Transport calculations were performed for Switzer and Arak realizations with spatial scale $\rho \in \{0.25, 0.5, 0.4\}$ and binary color fractions $p_\alpha \in \{0.3, 0.7\}$. Markov media corresponding to the Switzer procedure were sampled using the CASTOR code and particle transport was solved using the general-purpose TRIPOLI-4® Monte Carlo code developed at CEA [55]. For the Arak model, realizations were sampled using the POLLUX code and particle transport was solved using a Monte Carlo mini-app with a special interface for dealing with particle tracking in Arak media. For both random media models, 2000 independent realizations were sampled, and for each realization transport was solved using 2×10^6 particles split into 400 replicas. The fiducial quantity is the ensemble-averaged particle flux

$$\langle \varphi(x) \rangle = \frac{1}{M} \sum_{i=1}^{M} \varphi_i(x) \tag{35}$$

along the x axis of the geometry, where φ_i is the flux estimated in the ith realization and M is the number of realizations for

the random media. The statistical uncertainty $\sigma_{\langle \varphi \rangle}$ affecting the average flux $\langle \varphi \rangle$ stems from both the dispersion of the realizations

$$\sigma_G^2(x) = \frac{1}{M} \sum_{i=1}^{M} \varphi_i^2(x) - \langle \varphi(x) \rangle^2, \tag{36}$$

and the dispersion

$$\sigma_\varphi^2(x) = \frac{1}{M} \sum_{i=1}^{M} \sigma_{\varphi_i}^2 \tag{37}$$

due the statistical uncertainty $\sigma_{\varphi_i}^2$ of Monte Carlo transport for each realization i [15]. Hence, the combined error estimate on the average flux is

$$\sigma_{\langle \varphi \rangle}^2(x) = \frac{\sigma_G^2(x)}{M} + \sigma_\varphi^2(x). \tag{38}$$

Observe that the track-length-based estimator used in TRIPOLI-4 for the Switzer media is more efficient than the simpler collision-based estimator used in the mini-app Monte Carlo for the Arak media.

Our simulation results are shown in Fig. 13, where we display the ensemble-averaged flux as well as its variance. The standard error of the variance was estimated using the bootstrap resampling available in the SciPy package [56]. The default bias-corrected and accelerated (BCa) method was used, together with 9999 resamples for each bin. It is apparent that for both the mean and the variance the number of samples was sufficient to obtain small statistical uncertainty, which is barely visible in the figure.

These findings clearly demonstrate that there is a systematic, albeit small, difference in the distribution of the flux between "equivalent" Arak and Poisson models, where equivalence has been established by choosing the model parameters in order to have the same chord length distributions. A slight difference can be observed in the mean value, but the effect is much more pronounced for the second central moment. As expected, the discrepancy is amplified by the amount of scattering in the problem. In perfectly absorbing Markov media, transport would effectively take place along straight lines (except for the reflections from the boundary); thus, it would be governed by the line-Markov property alone and no differences between Arak and Poisson models should be observed. This effect is partially demonstrated for the cases with $p_0 = 0.7$, where the difference is reduced significantly with respect to cases with $p_0 = 0.3$. The discrepancy between the two models also decreases for larger ρ; however, this is not the case for the variance, where some significant offset remains.

VI. CONCLUSIONS

Several applications occurring in engineering and life sciences involve particle transport in disordered media: such materials, whose spatial features are known only statistically, are often described using various models borrowed from the theory of stochastic geometry. In this respect, random media whose line transects have a Markov property play a prominent role, in that they can be fully characterized by assigning two single parameters, the typical spatial scale and the coloring
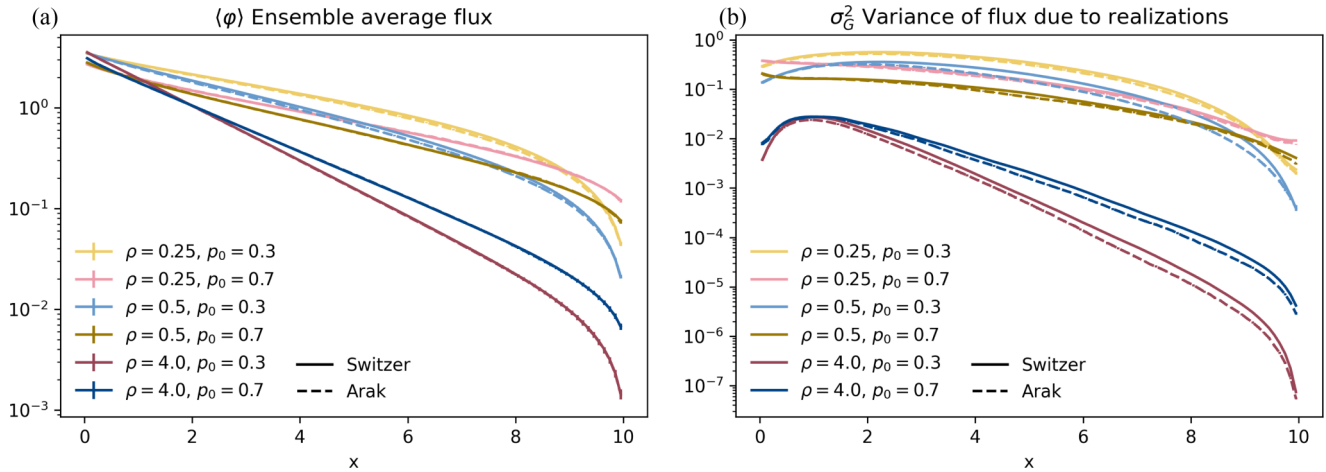
FIG. 13. Comparison of the ensemble-averaged particle flux and ensemble-averaged flux variance for a benchmark problem of particle transport in spatially homogeneous Switzer and Arak media with the same scale and color probability, for which the chord length distributions are identical. Two-dimensional realizations have been extruded in the z axis. Error bars (barely visible) correspond to one σ statistical uncertainty. The standard error of the variance was obtained by bootstrap.

probability. In this work, we have investigated the behavior of several homogeneous and nonhomogeneous random media exhibiting a Markov property, and their impact on the observables related to particle transport.

After reviewing the prototype case of one-dimensional Markov media on the line, we have considered the case of higher dimensions, which is mandatory to address real-world systems. A first generalization has been presented based on the Switzer procedure, where (generally nonhomogeneous) d-dimensional Poisson tessellations are randomly colored assigning each polyhedron a color with independent and spatially homogeneous probabilities: the resulting random media exhibit a line-Markov property. However, contrary to the one-dimensional case, where the sweeping procedure enables separately imposing spatial gradients in the spatial scale as well as in the coloring probability, Markov media obtained from the Switzer procedure can only display spatial gradients in the spatial scale.

In order to overcome this limitation, we have then examined the broad family of the Arak models, which can be used to sample two-dimensional random media exhibiting a stronger spatial Markov property, in addition to the line-Markov property. For the special case that we have selected in this paper, the only free parameters of the model are again the typical spatial scale and the coloring probability. Although their sampling strategy is much more cumbersome than in the case of the Switzer procedure, Arak models have an increased flexibility and allow for spatial gradients in the spatial scale as well as in the coloring probability.

A comparison of particle transport in Switzer-based and Arak-based Markov media for a few benchmark configurations consisting in binary mixtures of absorbing and scattering materials has shown that small but significant discrepancies appear in the ensemble-average particle flux through the geometries, despite the fact that both models were tuned so to share the same colored chord length distribution. The observed discrepancies, which are physically due to higher-order correlations between the particle trajectories and the spatial distribution of the material chunks (not fully captured by the chord distribution alone), increase with increasing scattering-to-absorption probability, and disappear entirely in the case of purely absorbing media. To the best of our knowledge, this is the first time that such a comparison has been attempted in the context of particle transport problems.

Future work will aim at extending our findings in several directions. Our analysis of the nonhomogeneous Arak model has been mainly driven by Monte Carlo simulations, and significant efforts would be needed in order to derive analytical results for the key statistical features, most importantly the line transect distributions as a function of the nonstationary event rates. Furthermore, the Arak model examined here is actually a special case of a very broad family of stochastic media with a spatial Markov property that can be obtained by properly tuning an additive potential $F(\omega)$ and sampling the corresponding particle dynamics: the effects of the resulting spatial patterns on particle transport clearly deserve to be investigated. A highly nontrivial question concerns the generalization of Arak models to dimension $d = 3$: the construction based on MCMC can be in principle carried over to higher dimensions, but the computational cost is likely to become unbearable; conversely, the particle dynamics construction, despite some promising preliminary results, seems to be still hindered by serious theoretical issues [57]. Finally, while our main focus has been on comparing Switzer-based and Arak-based random media, it would be interesting to further extend our investigation of particle transport to other models with a line-Markov property that are known in the literature, such as the iteration stable tessellations (STIT) [58].

[1] S. Torquato, *Random Heterogeneous Materials: Microstructure and Macroscopic Properties* (Springer, New York, 2002)

[2] G. C. Pomraning, *Linear Kinetic Theory and Particle Transport in Stochastic Mixtures* (World Scientific, Singapore, 1991).

[3] C. Levermore, G. Pomraning, D. Sanzo, and J. Wong, Linear transport theory in a random medium, J. Math. Phys. **27**, 2526 (1986).

[4] G. Viciconte, B.-J. Gréa, F. S. Godeferd, P. Arnault, and J. Clérouin, Sudden diffusion of turbulent mixing layers in weakly coupled plasmas under compression, Phys. Rev. E **100**, 063205 (2019).

[5] G. C. Pomraning, Radiative transfer in Rayleigh-Taylor unstable ICF pellets, Laser Part. Beams **8**, 741 (1990).

[6] J.-F. Clouet, F. Golse, R. Sentis, and M. Puel, On the slowing down of charged particles in a binary stochastic mixture, Kinetic Related Models **1**, 387 (2008).

[7] F. Malvagi, R. N. Byrne, G. C. Pomraning, and R. C. J. Somerville, Stochastic radiative transfer in partially cloudy atmosphere, J. Atmos. Sci. **50**, 2146 (1993).

[8] A. B. Davis and A. Marshak, Photon propagation in heterogeneous optical media with spatial correlations: Enhanced mean-free-paths and wider-than-exponential free-path distributions, J. Quant. Spectrosc. Radiat. Transfer **84**, 3 (2004).

[9] E. Kassianov and D. Veron, Stochastic radiative transfer in Markovian mixtures: Past, present, and future, J. Quant. Spectrosc. Radiat. Transfer **112**, 566 (2011).

[10] W. B. Doub, Particle self-shielding in plates loaded with spherical poison particles, Nucl. Sci. Eng. **10**, 299 (1961).

[11] M. Williams, The transmission of radiation through a spatially stochastic medium, J. Quant. Spectrosc. Radiat. Transfer **101**, 29 (2006).

[12] E. W. Larsen and R. Vasques, A generalized linear Boltzmann equation for non-classical particle transport, J. Quant. Spectrosc. Radiat. Transfer **112**, 619 (2011).

[13] C. Larmier, A. Zoia, F. Malvagi, E. Dumonteil, and A. Mazzolo, Neutron multiplication in random media: Reactivity and kinetics parameters, Ann. Nucl. Energy **111**, 391 (2018).

[14] A. Marinosci, C. Larmier, and A. Zoia, Neutron transport in anisotropic random media, Ann. Nucl. Energy **118**, 406 (2018).

[15] C. Larmier, F.-X. Hugot, F. Malvagi, A. Mazzolo, and A. Zoia, Benchmark solutions for transport in *d*-dimensional Markov binary mixtures, J. Quant. Spectrosc. Radiat. Transfer **189**, 133 (2017).

[16] C. Larmier, A. Lam, P. Brantley, F. Malvagi, T. Palmer, and A. Zoia, Monte Carlo chord length sampling for *d*-dimensional Markov binary mixtures, J. Quant. Spectrosc. Radiat. Transfer **204**, 256 (2018).

[17] G. Pomraning, Radiative transfer and transport phenomena in stochastic media, Int. J. Eng. Sci. **36**, 1595 (1998).

[18] D. W. Meyer and F. Saggini, Testing the Markov hypothesis in fluid flows, Phys. Rev. E **93**, 053103 (2016).

[19] M. Adams, E. Larsen, and G. Pomraning, Benchmark results for particle transport in a binary Markov statistical medium, J. Quant. Spectrosc. Radiat. Transfer **42**, 253 (1989).

[20] P. S. Brantley, A benchmark comparison of Monte Carlo particle transport algorithms for binary stochastic mixtures, J. Quant. Spectrosc. Radiat. Transfer **112**, 599 (2011).

[21] C. Deutsch and D. Vanderhaegen, Radiative transfer in statistically heterogeneous mixtures, J. Quant. Spectrosc. Radiat. Transfer **44**, 163 (1990).

[22] R. Sanchez, O. Zuchuat, F. Malvagi, and I. Zmijarevic, Symmetry and translations in multimaterial line statistics, J. Quant. Spectrosc. Radiat. Transfer **51**, 801 (1994).

[23] P. S. Brantley, P. F. O'Rourke, and A. K. Prinja, Verification of a Monte Carlo Levermore-Pomraning algorithm for spatially-inhomogeneous binary stochastic media, in *Proc. M&C 2019* (American Nuclear Society, Portland, OR, 2019), pp. 2067–2078.

[24] R. Sanchez, Linear kinetic theory in stochastic media, J. Math. Phys. **30**, 2498 (1989).

[25] E. C. Pielou, The spatial pattern of two-phase patchwork of vegetation, Biometrics **20**, 156 (1964).

[26] M. Bartlett, A note on spatial pattern, Biometrics **20**, 891 (1964).

[27] P. Switzer, A random set process in the plane with a Markovian property, Ann. Math. Stat. **36**, 1859 (1965).

[28] T. Lepage, L. Delaby, F. Malvagi, and A. Mazzolo, Monte Carlo simulation of fully Markovian stochastic geometries, Prog. Nucl. Sci. Tech. **2**, 743 (2011).

[29] O. Haran, D. Shvarts, and R. Thieberger, Transport in two-dimensional scattering stochastic media: Simulations and models, Phys. Rev. E **61**, 6183 (2000).

[30] C. Larmier, E. Dumonteil, F. Malvagi, A. Mazzolo, and A. Zoia, Finite-size effects and percolation properties of Poisson geometries, Phys. Rev. E **94**, 012130 (2016).

[31] R. Schneider and W. Weil, *Stochastic and Integral Geometry* (Springer, Berlin, 2008).

[32] C. Larmier, A. Marinosci, and A. Zoia, Chord length distribution in *d*-dimensional anisotropic Markov media, J. Quant. Spectrosc. Radiat. Transfer **224**, 403 (2019).

[33] M. A. Kowalski, C. Larmier, F. Madiot, J. Durand, S. Lemaire, and A. Zoia, Particle transport in Markov media with spatial gradients: Comparison between reference solutions and chord length sampling, J. Quant. Spectrosc. Radiat. Transfer **286**, 108185 (2022).

[34] T. Arak, On Markovian random fields with finite number of values, in *4th USSR-Japan Symposium on Probability Theory and Mathematical Statistics, Abstracts of communications* (Tbilisi, 1982).

[35] T. Arak and D. Surgailis, Markov fields with polygonal realizations, Probab. Theory Relat. Fields **80**, 543 (1989).

[36] T. Arak and D. Surgailis, Consistent polygonal fields, Probab. Theory Relat. Fields **89**, 319 (1991).

[37] T. Arak, P. Clifford, and D. Surgailis, Point-based polygonal models for random graphs, Adv. Appl. Probab. **25**, 348 (1993).

[38] D. T. Gillespie, Exact stochastic simulation of coupled chemical reactions, J. Phys. Chem. **81**, 2340 (1977).

[39] P. Clifford and R. D. Middleton, Reconstruction of polygonal images, J. Appl. Stat. **16**, 409 (1989).

[40] R. E. Miles, Random polygons determined by random lines in a plane, Proc. Natl. Acad. Sci. U. S. A. **52**, 901 (1964).

[41] R. E. Miles, The random division of space, Adv. Appl. Probab. **4**, 243 (1972).

[42] R. Schneider, Nonstationary Poisson hyperplanes and their induced tessellations, Adv. Appl. Probab. **35**, 139 (2003).

[43] A. Olson, S. Pautz, D. Bolintineanu, and E. Vu, Theory and generation methods for N-ary stochastic mixtures with Markovian mixing statistics, in *Proceedings of Mathematics & Computation (M&C) 2021* (American Nuclear Society, Raleigh, NC, 2021), pp. 258–269.

[44] N. P. Judish, Polygonal random fields and the reconstruction of piecewise continuous functions, Master's thesis, Massachusetts Institute of Technology, Cambridge, MA (1993).

[45] P. Clifford, Markov random fields in statistics, in *Disorder in Physical Systems. A Volume in honour of John M. Hammersley* edited by G. Grimmett and D. Welsh (Oxford University Press, Oxford, 1990), pp. 19–32.

[46] P. Clifford and G. Nicholls, A Metropolis sampler for polygonal image reconstruction, technical report, Department of Statistics, Oxford University (1995).

[47] T. Schreiber, Random dynamics and thermodynamic limits for polygonal Markov fields in the plane, Adv. Appl. Probab. **37**, 884 (2005).

[48] M. Paskin and S. Thrun, Robotic mapping with polygonal random fields, in *UAI '05, Proc. 21st Conference in Uncertainty in Artificial Intelligence, Edinburgh, Scotland, July 26–29, 2005*, edited by F. Bacchus and T. Jaakkola (AUAI Press, Arlington, Virginia, 2005), pp. 450–458.

[49] R. Kluszczyński, M.-C. van Lieshout, and T. Schreiber, An algorithm for binary image segmentation using polygonal Markov fields, in *Image Analysis and Processing—ICIAP 2005*, edited by F. Roli and S. Vitulano (Springer, Berlin, 2005), pp. 383–390.

[50] R. Kluszczyński, M.-C. van Lieshout, and T. Schreiber, Image segmentation by polygonal Markov fields, Ann. Inst. Stat. Math. **59**, 465 (2007).

[51] T. Schreiber and M.-C. van Lieshout, Disagreement loop and path creation/annihilation algorithms for binary planar Markov fields with applications to image segmentation, Scand. J. Stat. **37**, 264 (2010).

[52] M. van Lieshout, Discrete multicolor random mosaics with an application to network extraction, Scand. J. Stat. **40**, 734 (2013).

[53] I. Lux and L. Koblinger, *Monte Carlo Particle Transport Methods: Neutron and Photon Calculations* (CRC Press, Boca Raton, FL, 1991).

[54] P. A. W. Lewis and G. S. Shedler, Simulation of nonhomogeneous Poisson processes by thinning, Naval Res. Logistics Q. **26**, 403 (1979).

[55] E. Brun, F. Damian, C. Diop, E. Dumonteil, F. Hugot, C. Jouanne, Y. Lee, F. Malvagi, A. Mazzolo, O. Petit, J. Trama, T. Visonneau, and A. Zoia, TRIPOLI-4®, CEA, EDF and AREVA reference Monte Carlo code, Ann. Nucl. Energy **82**, 151 (2015).

[56] P. Virtanen *et al.*, SciPy 1.0: Fundamental algorithms for scientific computing in Python, Nat. Methods **17**, 261 (2020).

[57] T. Schreiber, A polyhedral Markov field—Pushing the Arak-Surgailis construction into three dimensions, Markov Processes and Related Fields **12**, 43 (2006).

[58] W. Nagel and V. Weiss, Crack STIT tessellations: Characterization of stationary random tessellations stable with respect to iteration, Adv. Appl. Probab. **37**, 859 (2005).